Grazing incidence XAFS spectroscopy of uranyl sorbed onto TiO_2 rutile surfaces

C. Den Auwer,[a] R. Drot,[b] E. Simoni,*[b] S. D. Conradson,[c] M. Gailhanou[d] and J. Mustre de Leon[e]

[a] *CEA Marcoule DEN/DRCP/SCPS, 30207, Bagnols sur Cèze Cedex, France*
[b] *Institut de Physique Nucléaire, Université Paris Sud Orsay, 91405, Orsay Cedex, France*
[c] *Los Alamos National Laboratory, MST Division, PO Box 1663, MS G755, Los Alamos NM 87545, USA*
[d] *Laboratoire pour l'Utilisation du Rayonnement Electromagnétique, Université Paris Sud Orsay, 91898, Orsay Cedex, France*
[e] *CINVESTAV Departmento de Fisica Aplicada, Merida A.P. 73 Cordemex, C.P. 97310, Mexico*

Received (in Strasbourg, France) 8th October 2002, Accepted 28th October 2002
First published as an Advance Article on the web 14th January 2003

The surface complex formed by uranyl oxocations sorbed onto rutile titanium oxide has been probed by X-ray Absorption Spectroscopy. These measurements are part of a work that aims to model the interaction between heavy metal ions and mineral surfaces in aqueous conditions. In order to define the orientation and structure of the oxocation complex on the surface, both polycrystalline and monocrystalline (110) and (001) planes of rutile TiO_2 have been investigated. Polarized XANES measurements show that the uranyl rod sorbs nearly parallel to the rutile surface, although this ideal configuration must be modulated by the surface topographic defects. Site by site simulation compared to the EXAFS data suggests that two surface oxygen sites are involved: shared edge and shared summit oxygen atoms of the TiO_6 octahedron. Both grazing incidence EXAFS on the (110) plane and isotropic EXAFS on polycrystalline TiO_2 reveal comparable sorption behavior: on average, the uranyl oxocation bonds to the surface as a bidentate complex with two short oxygen distances at 2.32 Å and three larger distances at 2.47 Å. Grazing incidence EXAFS on the (001) plane shows an unexpected low signal to noise ratio due to the lower uranium uptake. Data analysis suggests the formation of an outer sphere uranium complex on this plane. The discrepancy between both plane reactivities is still not understood.

Introduction

Among various environmentally relevant phenomena, the migration of radionuclides potentially released from geological waste disposal is of great importance.[1] Sorption and precipitation/solubility of radionuclides[2–6] are the most important factors determining their retention. Indeed, the fate of the radionuclides potentially released is usually evaluated by the partition between a mobile dissolved phase and a precipitated or sorbed phase. Therefore, it is necessary to model the radionuclide migration through numerous natural minerals in order to assess the performance of the confinement of the underground nuclear waste repository. A specific example of this problem is the remediation of facilities, sediments, and soils contaminated with uranium.[7,8]

In order to model the interactions between heavy metal ions and mineral surfaces in aqueous media, detailed knowledge of the physico-chemical reactions at the solid–solution interface is required. These interfacial reactions depend mainly on several geochemical parameters such as pH, redox potential and ionic strength of the aqueous medium, the speciation of the metal ion and the surface properties of the substrates (acidity and surface site density), which make a quantitative description rather complicated. Nevertheless, the macroscopic thermodynamics do not give any accurate information about the elementary chemical reactions used to determine the equilibrium constants. With ion exchange or surface complexation models, the simulations of the macroscopic experimental data do not give unambiguous results and could yield, without any experimental validation, arbitrary surface complexes.[9–11] Thus, it is necessary to relate the expected surface complexes to the structure of the surface coordination complexes. Therefore, the stoichiometry of the chemical species involved in such processes should be deduced from molecular-scale information provided by spectroscopic investigations. In addition, these molecular studies emphasize the fact that the sorbed ion size and the structure of the surface involved are parameters as important as the geochemical ones. Molecular probes thus constrain the equilibrium thermodynamic simulations of the retention data. Consequently, the mechanistic understanding will provide high confidence in the prediction of the fate and the transport of metal ions in natural systems. X-Ray Absorption Spectroscopy (XAS) is one of the techniques that has been successfully applied to this problem. Its use in actinide physical chemistry has been constantly growing for the past fifteen years in the fields of environmental studies related to the nuclear waste issue. Considering sorption and related phenomena, although the uranium cation has been most extensively investigated among the actinide family,[12–20] recent works have also been devoted to neptunium,[21,22] thorium[23] and americium sorption behavior.[24] Among the questions that XAS has addressed are inner- *versus* outer-sphere complexation, formation of polynuclear precipitates, and mono- *versus* polydentate surface binding modes. Although one of the drawbacks of the technique is to average the signal over all the possible species, tentative site by site data analysis has been successfully undertaken. Some of the more recent studies[7,22,23] exemplify this method,

 DOI: 10.1039/b209961f

considering a topological approach between the cation coordination sphere and the surface. Thus, careful analysis of the backscattering paths originating from the substrate atoms allows the authors to draw the relationship between the actinide polyhedron and the substrate atoms. This relationship is often driven by thermodynamic equilibria such as pH. Note that for all these systems the surface species involved in the interface chemical reactions are difficult to measure due to their low concentration on the solid surface.

In this paper, we present the investigation of the local structure of uranyl ion (UO_2^{2+}) sorbed onto TiO_2 (rutile), both polycrystalline and oriented single crystal. This substrate has been chosen as a model oxide that frequently occurs in the environment and influences contaminant transport in groundwater. Titanium dioxide presents two different well-known crystallographic structures, rutile and anastase. The rutile phase was selected because of the simplicity of the crystallographic atomic arrangement. It is composed of chains of slightly distorted Ti octahedra with alternate shared edge or shared corner connections within each chain. As a result, two types of oxygen sites are available for coordination, as described in the course of this article. Three substrates were considered for this article: polycrystalline rutile and the (110) and (001) crystallographic planes. A combination of conventional XAS measurements and polarized grazing incidence XAS resulted in the topographical approach described above.

Experimental

Sample preparation

Titania powder (rutile structure) as well as single crystals were purchased from CERAC. For the powder, the chemical purity is 99.5% with an average grain size lower than 75 μm and a specific surface area equal to 4.9 $m^2\ g^{-1}$ (measured by the N_2-BET method). Prior to the experiments, surface impurities were removed by washing the solid using deionized water until a constant electrical conductivity was reached.

The dimensions of titania single crystals in the (110) orientation is 10 mm × 10 mm and 1 mm thick. The uranium(VI) stock solutions were prepared by dissolving solid uranyl perchlorate in a 0.5 M $NaClO_4$ solution previously acidified with $HClO_4$ in order to avoid cation hydrolysis. Solid uranyl perchlorate was obtained after several steps of dissolution and evaporation of $UO_2(NO_3)_2{\cdot}6H_2O$ (from MERCK) in $HClO_4$. Sorption experiments were performed at room temperature considering classical batch experiments in polypropylene tubes. Uranyl concentrations in solution were measured by α-liquid scintillation using a TRI-CARB 2700TR PACKARD spectrometer. The sorption protocol was slightly different for powder and crystal substrates.

U(VI)/TiO_2(p). A weighed amount (500 mg) was equilibrated for 24 hours (hydration step) with 10 mL of $NaClO_4$ (0.5 M) solution adjusted to pH = 3.5 with $HClO_4$ 5 M. The sample was then centrifuged and part of the liquid was replaced by U(VI) stock solution to get 10^{-3} M as the initial uranium concentration. Then, the suspension was shaken for 5 hours (sorption step) and after centrifugation the final uranyl concentration and the sorption rate were determined (about 35%). Considering the specific surface area of the titania powder and the above sorption conditions, the value of 35% for the sorption rate leads to less than 10^{18} uranium atoms m^{-2}. Thus we can reasonably assume that full surface coverage is not reached in our experimental conditions. The loaded solids were finally washed with small amounts of deionised water and dried at room temperature before XAS analysis.

U(VI)/TiO_2(110) and U(VI)/TiO_2(001). As we can expect that the sorption rate is faster than for powders, the sample was placed directly in 1 mL of uranyl solution (10^{-4} M; pH = 3). For single crystals, it could be very easy to reach a full saturated surface during sorption experiments and potentially form surface precipitates. In order to address this question the U 4f XPS signal of the studied sample was compared to that obtained for a sample prepared with 1 mL of a uranyl solution with 10^{-6} M uranium concentration and pH = 3 (comparable to the above powder sample which corresponds to unsaturated conditions). No difference was found between these samples which indicates that there is no surface site saturation for single crystals in our conditions. Moreover, this conclusion is corroborated by the absence of any U–U peak in the Fourier transform of the EXAFS oscillations, as will be discussed below.

U(VI)/aq. The 0.01 M uranium (VI) perchlorate solution was prepared from the U(VI) stock solution as described above.

XAS data

Data collection. Uranium L_{III} edge (17 166 eV) data were recorded at the following synchrotron facilities: U(VI)/TiO_2(p) at ESRF, ROBL beam line (Grenoble, France); U(VI)/TiO_2(110), U(VI)/TiO_2(001) and U(VI)/aq at SSRL, 11-2 beam line (Stanford, USA).

ROBL:[25] bending magnet. The ring was operated at 6.0 GeV with an optimal current of 200 mA. 11-2:[26] 26-pole wiggler. The ring was operated at 3.0 GeV with an optimal current of 100 mA.

The beam line monochromators were calibrated before and after the measurement using a Zr metallic foil (K edge at 17999.35 eV). Complete beam line descriptions have been provided elsewhere,[25,26] the following summarizes the beam line main components along the beam path.

ROBL: a set of vertical and horizontal slits, a vertical collimating mirror, a double crystal Si(111) monochromator, a vertical focussing mirror, a set of horizontal and vertical slits, I_0 ionization chamber, sample holder and fluorescence detection (4-element Ge detector). Beam line resolution at the U L_{III} edge: 4.3 eV. Scan parameters: pre-edge region (17 000–17 160 eV, 1s per 5 eV); post-edge region (17 160 eV–18 000 eV, 0.5 eV per 2 s). 4 scans.

11-2: a set of vertical slits, a vertical collimating mirror, a set of horizontal and vertical slits, a liquid nitrogen cooled Si(220) double crystal monochromator, a toroidal focussing mirror, a set of horizontal and vertical slits, I_0 ionization chamber filled with argon, sample goniometer for grazing incidence and fluorescence detection (30-element Ge array detector), I_1 ionization chamber filled with argon. The beam line was run focussed at the U L_{III} edge for the XANES measurements (beam line resolution at this edge: 1.2 eV) and unfocussed (to avoid beam unstability) for the EXAFS measurements. Scan parameters: pre-edge region (17 000–17 140 eV, 40 points, 1s per point); edge region (17 140 eV–3 k, 3s per 0.8 eV); EXAFS region (3 k–12 k, 3–10 s per 0.05 k). 25 scans.

The 3-axes goniometer has been described in detail elsewhere.[19a] The grazing incidence angle θ was obtained by maximizing the fluorescence signal, near the specular angle of TiO_2 at the U L_{III} edge energy (0.12°). For measurements with the polarization vector on the crystallographic plane (//), the tilt angle χ was set to 0° (horizontal crystal). For measurements with the polarization vector normal to the crystallographic plane (⊥), χ was set to 90° (vertical crystal). The EXAFS spectra of U(VI)/TiO_2(110) and U(VI)/TiO_2(001) were only recorded in the // position. As explained in the text, the ⊥ position does not allow a satisfactory signal to noise ratio. The fluorescence detection was carried out by selecting the U Lα1 emission line at 13 615 eV. Bragg diffraction peaks from

the crystal were avoided by seeking the optimum sample rotation ϕ angle.

Data analysis. Data were analyzed using the EXAFS98 code.[27] Pre-edge background removal was carried out on all spectra using a linear function. XANES spectra were normalized to an absorption equal to 1.0 at the middle of the first EXAFS oscillation (17 250 eV). EXAFS oscillations were normalized with respect to the atomic absorption (Lengeler–Eisenberger) modeled by a cubic spline function with 5 knots. Fourier transformation (FT) to real space was performed using k^3 weighting and a Kaiser window between 2.7 and 12.5 Å^{-1} with a spatial resolution of 0.16 Å. For U(VI)/TiO_2(001), due to the low signal to noise ratio, FT was performed between 2.7 and 10.0 Å^{-1}

Curve fitting. EXAFS data fitting was carried out with RoundMidnight code.[27] Sets of phases $\phi(\theta,k)$, amplitude $f(\theta,k)$ and electron mean free path $\lambda(k)$ functions were generated with Feff8.1 code[28,29] using two model clusters. Potential calculations inside the Feff code were carried out with self consistency within a cluster of 4.45 Å. Edge spectra were calculated with the full multiple scattering method inside a sub-cluster of 4.45 Å. EXAFS spectra were calculated using the path expansion approximation up to 6 Å

The first model cluster of a $UO_2(O)_5$ pentagonal bipyramid (PBP) was constructed to model the U(VI)/aq species: 2 O at 1.75 Å, 5 O at 2.50 Å. The reliability of ϕ, f, and λ obtained with this calculation and used to fit the data of U(VI)/aq was tested on the model compound $Cu[(UO_2)_2(SiO_3OH)_2]\cdot 6H_2O$ (cuprosklodowskite). Crystallographic parameters of the first coordination sphere:[30] 2 O at 1.77 Å, 3 O at 2.32 Å, 2 O at 2.43 Å. EXAFS best fit parameters: 2 O at 1.76(1) Å, 3 O at 2.32(1) Å, 2 O at 2.45(1) Å, r factor = 0.014.

The second model cluster of $UO_2(O)_3$ was positioned onto the (110) surface of the rutile crystal ($P4_2/mnm$, $a = b =$ 4.594, c = 2.958 Å), $UO_2(O)_3/TiO_2$(110): 2 O at 1.78 Å, 3 O at 2.44 Å, 2 O at 2.30 Å. As discussed in this article, two oxygen sites are present in this surface: bridging oxygen atoms corresponding to a Ti octahedron edge (site A) and non-bridging oxygen atoms corresponding to two Ti octahedron summits (site B). Two models were therefore constructed on the (110) surface, one involving two bridging surface oxygen atoms and one involving two non-bridging surface oxygen atoms. In both cases, the uranium atom is bidentate with respect to the surface. The ϕ, f and λ functions obtained with model A site (electronic parameters corresponding to site B are identical, except for the U···Ti contribution) were used to fit the data of U(VI)/TiO_2(p), U(VI)/TiO_2(110) and U(VI)/TiO_2(001). Their reliability was also tested on model compound $Cu[(UO_2)_2(SiO_3OH)_2]\cdot 6H_2O$ (cuprosklodowskite). EXAFS best fit parameters: 2 O at 1.78(1) Å, 3 O at 2.31(1) Å, 2 O at 2.41(1) Å, r factor = 0.013.

Fitting procedure was carried out in $k\chi(k)$ for the filtered back-transformed EXAFS oscillations between 0.7 and 4.0 Å (0.7 to 2.2 Å for U(VI)/TiO_2(001)). No significant signal is included in the spectra beyond 4 Å and the back-Fourier transform operation suppresses the high frequency noise. The scattering paths included in the fit are described in the Results and Discussion section. The Debye–Waller factor of the quadrupole multiple scattering path of O=U=O′ was fixed to two times that of the U=O single scattering path.[31] Empirical self-absorption and dead time corrections were obtained by normalizing the EXAFS first shell amplitude to two oxygen atoms (this is always the case for U(VI) in aqueous media). Although self-absorption is expected to be small for the sorbed samples, dead time corrections might become significant as the integrated count rate of the detector was set at high values (the ratio ICR/U(Lα1)CR was about 1000). Global absorption correction factors were included in the floating S_0^2 parameter and were found to be equal to 1.223 for U(VI)/aq, 0.958 for U(VI)/TiO_2(p), 0.951 for U(VI)/TiO_2(110) and 1.206 for U(VI)/TiO_2(001).

Results and discussion

Grazing incidence XANES

In order to address the orientation and structure of the oxocation complex onto the surface, the three rutile samples that have been considered in this study, (U(VI)/TiO_2(p), U(VI)/TiO_2(110) and U(VI)/TiO_2(001)), are expected to give complementary answers. In the polycrystalline case, and because the XAFS probe averages over all the central atom crystallographic sites, a convoluted signal over the different surface complexes is expected. In the crystal surface investigation, because of the sample anisotropy and by use of the polarized X-ray beam, the oxocation orientation, if any, is expected to be defined as well as the topographic relationship between the uranyl and the Ti octahedra.

The L_{III} absorption edge of uranium arises from the excitation of a $2p_{3/2}$ core electron to the vacant 6d orbitals (major transition in the dipolar approximation).[32] Fig. 1a shows the uranium L_{III} XANES spectra of compounds U(VI)/aq, U(VI)/TiO_2(p) and U(VI)/TiO_2(110). The broad white line **A** is typical for uranyl L_{III} edge (2p core hole width = 7.4 eV[33]). Note that **A** is less intense in the case of U(VI)/TiO_2(p) than in the other cases. Comparison with other measurements carried out on these beam lines shows that the experimental energy resolution is responsible for this discrepancy in **A** intensity. At this edge, the uranyl XANES spectrum is well known to exhibit a characteristic feature (about 17 eV above the edge maximum) accounting for a strong multiple scattering contribution due to the linear oxocation bonds.[31,34–36] All the spectra of Fig. 1a, as expected in such sorption conditions, exhibit the uranyl characteristic feature, **B**, and its occurrence is discussed below in more details. Feature **C** accounts for the second sphere backscattering neighbors. The high energy shift (about 1 eV) of **C** in Fig. 1a from U(VI)/aq to U(VI)/TiO_2(p) and U(VI)/TiO_2(110) suggests a small contraction of the uranium second coordination sphere upon sorption.

The two non-polarized (isotropic) simulations of $UO_2(O)_5$ pentagonal bipyramid (PBP) and $UO_2(O)_3/TiO_2$(110) (site A case) reproduce qualitatively the experimental spectra (*cf.* Fig. 1). However, feature **C** is more pronounced in the experimental spectrum of U(VI)/aq than in the calculated PBP one. This might be attributed to the fact that the effect of the solvant medium is not properly taken into account in the simulation of an isolated PBP cluster.

Although the polarization dependence of the K or L_I edges depends on a factor that ranks from 3 to 0 (from parallel to perpendicular relative angle between the X-ray electric field vector $\hat{\varepsilon}$ and the bond vector $\hat{r}$)[31] this is not the case for the L_{II}, L_{III} edges for which the effect is much weaker. After the work of Citrin,[37] the effective number of neighbors can be approximated by the relation:

$$N_{\mathrm{eff}}(\theta) = \sum_{i=1}^{N} (0.7 + 0.9|\hat{\varepsilon}\cdot\hat{r}|) \qquad (1)$$

where N is the number of neighbors at r and $\hat{\varepsilon}\cdot\hat{r}$ is the scalar product of the X-ray electric field vector with the bond vector. From a parallel to perpendicular relative orientation of $\hat{\varepsilon}$ and $\hat{r}$, the factor in brackets in eqn. (1) varies from 1.6 to 0.7.

Unfortunately, the K edge of uranium is energetically out of range and the L_I edge absorption cross section and fluorescence emission line are far weaker than the L_{III} ones, making the measurements extremely difficult on highly dilute systems.

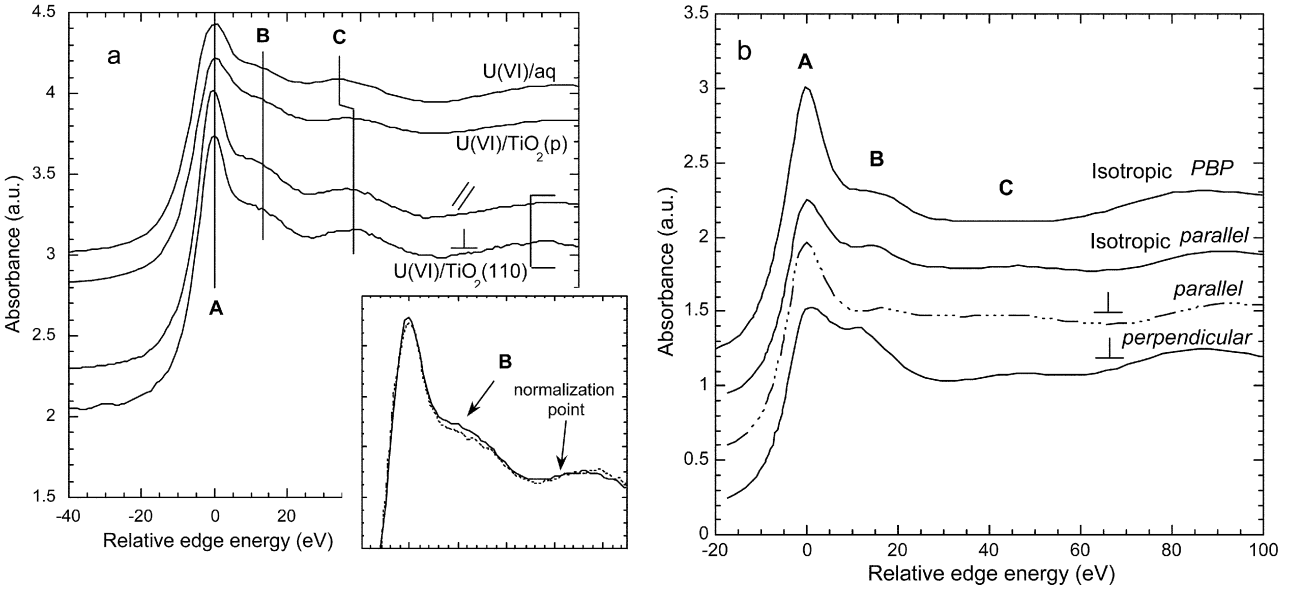

Fig. 1 a) Uranium L_{III} edge experimental spectra of U(VI)/aq, U(VI)/TiO_2(p) and U(VI)/TiO_2(110). U(VI)/aq and U(VI)/TiO_2(p) correspond to isotropic measurements. U(VI)/TiO_2(110) was measured with $\hat{\varepsilon}$ parallel (middle curve) and perpendicular (bottom curve) to the (110) surface. For clarity, spectra have been shifted along the ordinate axis and energy was calibrated against the absorption white line maximum. b) Uranium L_{III} edge simulated spectra (Feff8.1) of $UO_2(O)_5^{2+}$ and $UO_2(O)_5$ clusters on the TiO_2(110) surface in the parallel and perpendicular configurations of the oxocation with respect to the surface. The simulation assumes non-polarized X-rays (top curve) or was carried out with $\hat{\varepsilon}$ normal to the surface (bottom curves).

The Fourier transformed intensity of the EXAFS oscillations (and in particular the contribution from the uranyl oxygen atoms) is expected to be highly sensitive to the polarization effect.[31] Unfortunately with $\hat{\varepsilon}$ normal to the crystal plane the crystal intercepts the beam horizontally, thus lacking a factor of 100 in the photon flux on the sample. No EXAFS data could be recorded in this configuration. Thus using the polarized XANES technique and observing the evolution of the oxocation characteristic **B** feature, two ideal configurations must be distinguished:

i) The uranyl rod is parallel to the surface: with $\hat{\varepsilon}$ normal to the crystal surface, $N_{eff}(\perp)$ is given by $N_{eff} = 1.4$ and **B** must decrease in intensity with respect to $N = 2$. With $\hat{\varepsilon}$ parallel to the surface, $N_{eff}(//)$ is averaged over the 360° in plane orientations and this case is equivalent to the isotropic one ($N_{eff} = N = 2$).

ii) The uranyl rod is perpendicular to the surface: with $\hat{\varepsilon}$ normal to the crystal surface, $N_{eff}(\perp) = 3.2$. With $\hat{\varepsilon}$ parallel to the surface, $N_{eff}(//) = 1.4$.

Fig. 1b shows the L_{III} edge XANES simulations of an actinyl pentagonal complex positioned with the actinyl rod parallel and perpendicular to the rutile (110) surface. The simulation compares the isotropic case to configurations i) and ii) for which $\hat{\varepsilon}$ is normal to the (110) plane. In the first case, although much smaller than previously described,[31,34,38] a decrease of **B** intensity can be observed. In the second case, **B** is strongly increased. Note that the energy of **B** evolves from one orientation to another because the backscattering phase is sensitive to the electric field direction. Comparison of these simulations with the experimental spectra of Fig. 1a demonstrates that the uranyl rod is not perpendicular to the surface in U(VI)/TiO_2(110). This result is expected because the two axial oxygen atoms are too strongly bonded to the uranium to be available for any coordination with the surface. Although the polarization effect on **B** has been proved small by the simulation when the oxocation is parallel to the surface, it can be hardly seen in the experimental spectra. This is attributed to the topography of the surface that exhibits steps, plateaux and defects instead of an ideal planar geometry.[39] It averages the uranyl orientation to a value higher than the ideal 0 degrees corresponding to perfect parallelism. As a result of this effect the decrease of **B** intensity in the perpendicular configuration is much smaller than expected from the simulation, as observed in Fig. 1a.

Grazing incidence EXAFS

Fig. 2a presents the raw EXAFS spectra of U(VI)/aq and Fig. 2b shows the corresponding FT. The structural parameters presented in Table 1 obtained for U(VI)/aq agree well with the data previously reported in the literature.[40–45] Because of the back-FT range, the fit (Fig. 3) must include the four-legged multiple scattering path O=U=O′. Its path length was fixed as twice the first shell U=O bond length. Further addition of the three-legged O=U=O′ and four-legged O=U=O scattering paths did not improve the fit quality, as already reported.[7,31] Difference shell analysis was performed by substraction of U=O and O=U=O contributions from $k\chi(k)$. The resulting $k\chi(k)^{eq}$ corresponding to the uranium equatorial shell displayed in Fig. 4 shows that the second uranium neighbors (the equatorial oxygen atoms) behave as a pure single distance oscillator as can be expected for the aqueous uranyl species. Therefore the uranyl cation environment in aqueous media is best described as a pentagonal bipyramid.

The modification of the beating in the raw EXAFS signal between 6 and 9 $Å^{-1}$ from aqueous to sorbed uranyl suggests a distortion of the pentagonal bipyramid polyhedron upon sorption onto the rutile surface. The rutile structure is composed of strings of Ti cations surrounded by slightly distorted shared-edge oxygen octahedra. Two types of oxygen atoms from the Ti polyhedra are available for surface coordination: bridging oxygen atoms corresponding to an octahedron edge (site A) and non-bridging oxygen atoms corresponding to two octahedra summits (site B). As an example, Fig. 5 presents the (110) crystallographic plane of TiO_2 which contains 50% of site A and 50% of site B. In contrast, the (001) plane contains 100% of site A. In the polycrystalline rutile sample, all the crystallographic planes are present, although in a proportion that is unknown, and this leads to an averaging of site A type and site B type occurrences. In order to better

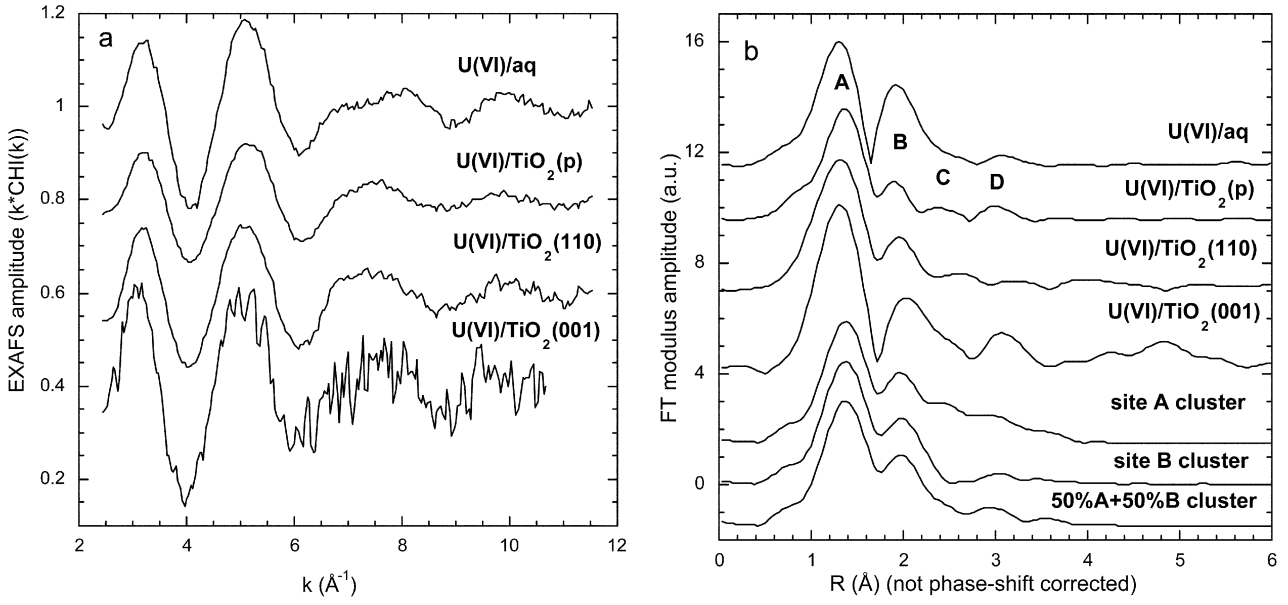

Fig. 2 a) Experimental raw EXAFS oscillations of U(VI)/aq, U(VI)/TiO_2(p), U(VI)/TiO_2(110)$_{//}$ and U(VI)/TiO_2(001)$_{//}$. For clarity, oscillations have been shifted along the ordinate axis. b) Experimental FT moduli of the EXAFS oscillations of U(VI)/aq, U(VI)/TiO_2(p), U(VI)/TiO_2(110)$_{//}$ and U(VI)/TiO_2(001)$_{//}$. Comparison is made with the simulated spectrum of the $UO_2(O)_3$ cluster on the TiO_2(110) surface (site A, B, 50% site A + 50% site B). For clarity, moduli have been shifted along the ordinate axis.

understand the relation between the oxocation and the surface oxygen sites, two clusters of $UO_2(O)_3/TiO_2$ have been constructed as site A and site B surface complexes (see Experimental section for details). In both cases, the axial and equatorial uranium coordination shells are identical since the two surface O–O distances in site A and site B are identical (2.96 Å), yielding the same equatorial shell geometry for both sites. However the two complexes differ in their third coordination sphere, as a consequence of the Ti position. Fig. 2b presents the simulated FT spectra of site A and B complexes. The two simulations show that both sites can be differentiated and this can be explained using the description of the U backscattering paths. Although in both sites the U–O nearest scatters are identical, differences arise from the presence in site A of a U···Ti pair (around 3 Å). In site B, the U–O–Ti angle (around 140°) damps the U–O–Ti path amplitude, resulting in an insignificant contribution. One should note that the interference of the backscattering paths in the 2.2–3.4 Å range (not phase-shift corrected) of the FT makes inaccurate the direct assignment of one peak to one contribution (only used to seek clarity in the discussion). For instance peak C of the FT can be mainly attributed to the U···Ti interaction although it is mixed with the multiple scattering contributions of the *trans*-dioxo ion (peak D on the FT). The net result is a mixing of peaks C and D with modulations in amplitude. Because of the absence of any U–Ti path in site B, there is a minimum in the FT amplitude between 2.4 and 2.6 Å. An equal mixture of sites A and B was examined in order to simulate the presence of both sites in the polycrystalline and the (110) plane samples. This model is based on two assumptions: i) both sites are crystallographically present in the same proportion (this is true for the (110) plane but it depends on the preferred cleavage planes for the polycrystalline sample, and this is unknown); ii) both sites have comparable reactivity (this has not been demonstrated). The result of this simulation is shown at the bottom of Fig. 2b.

In a first approximation, a fit with one equatorial shell was carried out on U(VI)/TiO_2(p), U(VI)/TiO_2(110)$_{//}$ and U(VI)/TiO_2(001)$_{//}$. In the first two cases the back-FT range includes the U···Ti contribution from site A and the multiple scattering contribution from the *trans*-dioxo group as for U(VI)/aq. As an example, Fig. 6 shows the different scattering path contributions to the total EXAFS spectrum in the case of U(VI)/TiO_2(p). Note that no polarization effect is to be expected between U(VI)/TiO_2(p) and U(VI)/TiO_2(110)$_{//}$ or U(VI)/

Table 1 Best fit parameters of the filtered EXAFS oscillations of U(VI)/aq, U(VI)/TiO_2(p), U(VI)/TiO_2(110) and U(VI)/TiO_2(001)

Sample	Number of neighbors	U–O distances/Å	Debye–Waller/ Å^2; e_0/eV	*r* Factor
U(VI)/aq	*2.0*(−)[a] O	1.77(1)	σ^2 = 0.0038(1)	0.021
	4.7(3) O	2.42(1)	σ^2 = 0.0085(1)	
	2.0(−) O	3.54(−)	σ^2 = *0.0076*(−)	
			e_0 = −2.76(24)	
U(VI)/TiO_2(p):	*2.0*(−) O	1.79(1)	σ^2 = 0.0034(1)	0.030
one equat. shell	5.0(7) O	2.39(2)	σ^2 = 0.0175(15)	
	0.5(−) Ti	*3.13*(−)	σ^2 = 0.0400(350)	
	2.0(−) O	*3.58*(−)	σ^2 = *0.0068*(−)	
			e_0 = −2.24(49)	
two equat. shells	*2.0*(−) O	1.79(1)	σ^2 = 0.0035(1)	0.022
	2.5(4) O	2.33(2)	σ^2 = 0.0088(2)	
	3.1(1) O	2.49(3)	σ^2 = 0.0199(7)	
	0.5(−) Ti	*3.05*(−)	σ^2 = 0.0400(350)	
	2.0(−) O	*3.58*(−)	σ^2 = *0.0070*(−)	
			e_0 = −2.10(113)	
U(VI)/TiO_2(110):	*2.0*(−) O	1.78(1)	σ^2 = 0.0017(1)	0.019
one equat. shell	4.9(1) O	2.38(1)	σ^2 = 0.0115(1)	
	0.5(−) Ti	*3.12*(−)	σ^2 = 0.0324(40)	
	2.0(−) O	*3.56*(−)	σ^2 = *0.0034*(−)	
			e_0 = −3.57(12)	
	2.0(−) O	1.78(1)	σ^2 = 0.0014(1)	0.017
two equat. shells	2.1(2) O	2.31(1)	σ^2 = 0.0037(1)	
	2.9(2) O	2.46(1)	σ^2 = 0.0070(1)	
	0.5(−) Ti	*3.02*(−)	σ^2 = 0.0256(50)	
	2.0(−) O	*3.56*(−)	σ^2 = *0.0028*(−)	
			e_0 = −3.18(20)	
U(VI)/TiO_2(001)[b]:	*2.0*(−) O	1.77(1)	σ^2 = 0.0008(4)	0.028
one equat. shell	5.5(14) O	2.43(2)	σ^2 = 0.0107(3)	
			e_0 = −3.33(100)	

[a] Numbers in italics correspond to fixed or linked variables. [b] Because of the low signal to noise ratio of this spectrum, only a two-shell fit on a smaller back FT range was carried out (*cf.* Experimental section).

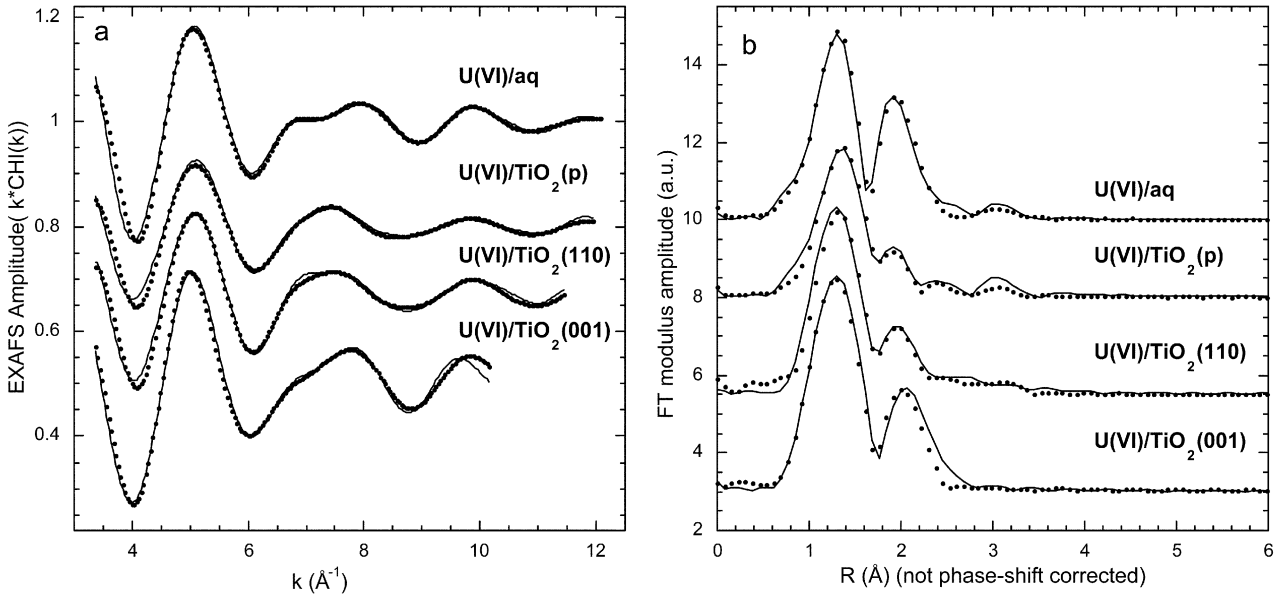

Fig. 3 a) Fitted (···) filtered EXAFS oscillations of U(VI)/aq, U(VI)/TiO_2(p), U(VI)/TiO_2(110)$_{//}$ and U(VI)/TiO_2(001)$_{//}$. For clarity, oscillations have been shifted along the ordinate axis. b) Corresponding fitted (···) FT moduli of the EXAFS oscillation of U(VI)/aq, U(VI)/TiO_2(p) U(VI)/TiO_2(110)$_{//}$ and U(VI)/TiO_2(001)$_{//}$. For clarity, FTs have been shifted along the ordinate axis.

TiO_2(001)$_{//}$ since the polarized XANES measurements have demonstrated that the angle between the surface and the uranyl axis is small. Because the signal to noise ratio is unexpectedly low for U(VI)/TiO_2(001)$_{//}$, only a reduced back-FT region including the first oxygen neighbors has been fit (*cf.* Experimental section). Given the above assumptions to define the ratio of site A and B in the (110) face and in the powder, the number of Ti atoms has been fixed to 0.5 in the fits. The U···Ti distance has also been linked to the U–O^{eq} distance given the geometrical constraints. The results for U(VI)/TiO_2(p) and U(VI)/TiO_2(110)$_{//}$ show a slight increase in the U=O bond distance (+0.02 Å) and a decrease in the U–O^{eq} bond distance (−0.03 Å) with respect to U(VI)/aq. However, these variations lie within the uncertainties of the measurements and they don't account for the beating modifications observed in the raw EXAFS spectra. Although the fit quality is satisfactory, the intensity decrease of peak B in the FT from U(VI)/aq to U(VI)/TiO_2(p) and U(VI)/TiO_2(110)$_{//}$ suggests a possible splitting of the second coordination shell, given that the usual number of equatorial neighbors for uranyl(VI) oxoanion is between 5 and 6. The difference shell analysis of Fig. 4 shows the equatorial backscatter oscillators. Clearly, a beating around 9.5 $Å^{-1}$ for U(VI)/TiO_2(p) and U(VI)/TiO_2(110)$_{//}$ suggests that two distances are included in this shell with a distance separation of ~0.16 Å (estimated from the beat-node position $k = \pi/(2\Delta R)$).

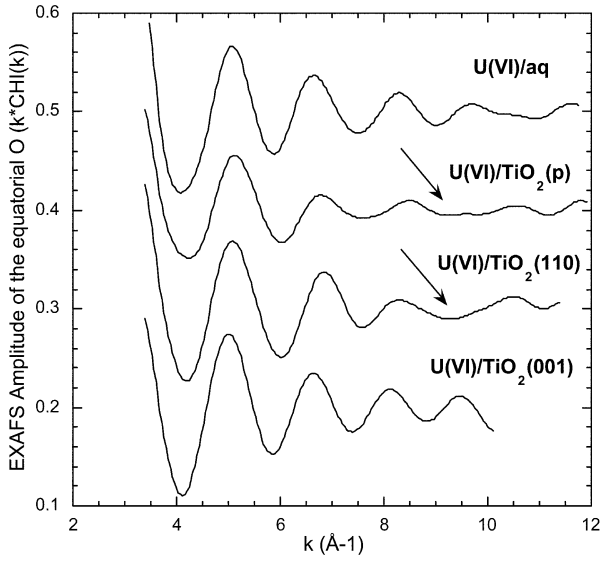

Fig. 4 Difference shell analysis of the filtered EXAFS oscillations of U(VI)/aq, U(VI)/TiO_2(p), U(VI)/TiO_2(110)$_{//}$ and U(VI)/TiO_2(001)$_{//}$ presenting the oscillations accounting for the equatorial oxygen atoms. The arrows show the beating in the EXAFS oscillation for U(VI)/TiO_2(p) and U(VI)/TiO_2(110)$_{//}$.

In the case of U(VI)/TiO_2(001)$_{//}$, the results of the fit with one equatorial shell are identical to those of U(VI)/aq, suggesting that another sorption mechanism is involved for this crystallographic face. Fig. 4 also shows that the equatorial shell most likely involves a single bond length, as no beating is visible. This suggests the formation of an outer-sphere complex in the case of the (001) surface and inner-sphere complex in the case of the (110) surface and the powder. However, this conclusion regarding the coordination of UO_2^{2+} when adsorbed onto the (001) surface must be drawn with some care, considering the small fitting range used and the low signal to noise ratio of the spectrum.

A similar fitting procedure with a split in the equatorial shells of U(VI)/TiO_2(p) and U(VI)/TiO_2(110)$_{//}$ yielded a short U–O distance (around 2.32 Å with two atoms) and a long distance (around 2.47 Å with three atoms). Such behavior has already been reported by Waite *et al.*,[46] with attribution of the shorter distance to out of plane equatorial oxygen neighbors (O^{out}) and of the larger distance to surface equatorial oxygen (O^{surf}). As for Waite *et al.*, the geometrical constraint of the surface oxygens precludes the occurrence of a tridentate uranyl complex to the surface. The number of neighbors from Table 1 is consistent with the formation of a bidentate complex. However the large uncertainties associated with the amplitude variables in EXAFS do not allow us to discriminate between Waite's proposed geometry and an opposite geometry with the short U–O equatorial distance associated to surface oxygens. In our fits, attempts to include the U···Ti contribution at a distance corresponding to U–O^{surf} longer than U–O^{out} lead to significant disagreement in the region of peaks C and D of the FT.

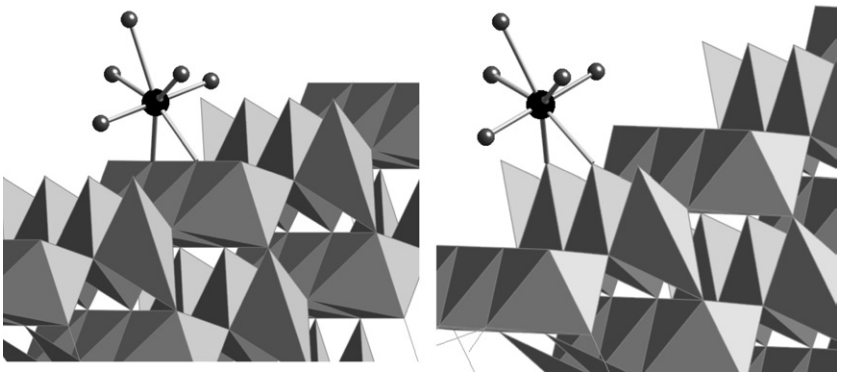

Fig. 5 a) $UO_2(O)_3$ cluster onto the $TiO_2(110)$ surface. Bridging oxygen atoms, site A. b) $UO_2(O)_3$ cluster onto the $TiO_2(110)$ surface. Non-bridging oxygen atoms, site B.

This suggests that in the case of titania, the U–O^{surf} bond lengths are shorter than the U–O^{out} bond lengths. In addition, this distance assignment is in better agreement with expected U–OH_2 distances in several uranyl compounds (above 2.4 Å).[47]

As a summary, Fig. 7 shows the schematic structure of the bidentate uranyl complex onto site A of the (110) surface. To date, the sorption behavior on the (001) surface leading to an outer-sphere complex is still not understood. Since this fit result is less credible because of the low signal to noise ratio of the spectrum, this result would suggest different reactivities for each surface. As a consequence, it would suggest that the assumption of equal site A and B occupation for the polycrystalline sample is probably too simplistic.

As previously noticed, a slight lengthening of the uranyl bond from 1.77 Å to 1.79 Å is also observed for U(VI)/TiO_2(p) and U(VI)/$TiO_2(110)_{//}$. This effect lies just above the uncertainty value. If significant, this 0.02 Å lengthening could be an indication of the covalency of the bond between the uranium atom and the surface oxygen atoms. Indeed, the length of the U–O^{ax} bond is related to the electronic density between these two atoms. Since the U–O^{ax} bond is longer, the density is lower, and as a rule of thumb it would be consistent with an increased covalency of the U–O^{surf} bond with respect to the aqueous species. The shortening of the U–O equatorial bond from 2.42 Å for U(VI)/aq to 2.32 Å for U–O^{surf} also favors this interpretation. This covalency in the U–O^{surf} bond is not surprising, taking into account the lack of coordination for the rutile surface oxygens and the possibility of charge delocalization along the surface.

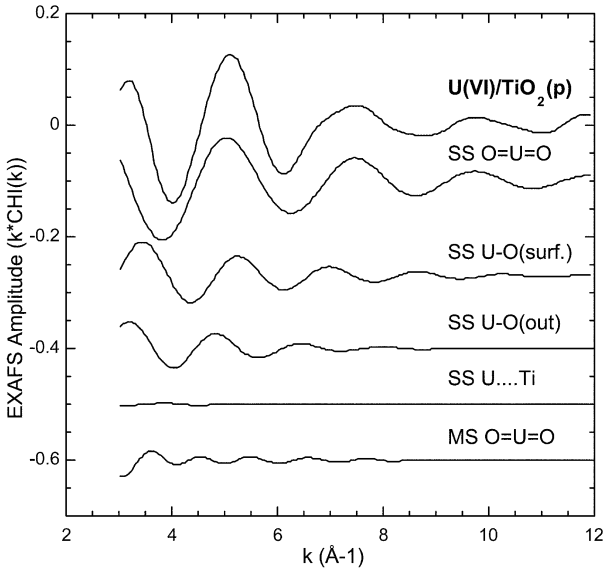

Fig. 6 Experimental filtered EXAFS oscillations of U(VI)TiO_2(p) and the 5 scattering paths included in the fitting procedure.

Conclusions

EXAFS and XANES measurements of the surface complex formed by uranyl sorbed onto TiO_2 rutile provide a complete description of the uranyl coordination sphere. Grazing incidence XAS has been used in order to define the orientation of the sorbed oxocation with respect to the surface as nearly parallel. EXAFS measurements in both isotropic and grazing incidence polarized modes have demonstrated that in both polycrystalline and monocrystalline (110) plane cases, the average structure of the surface complex results from a bidentate bonding mode to site A and B surface oxygen atoms. Addition of the U···Ti contribution from site A in the fits shows that the two short U–O equatorial distances correspond to surface binding and the three longer ones correspond to aquo oxygen atoms in order to complete the uranyl coordination sphere.

In the (001) plane case, an outer-sphere uranyl complex is formed, in contrast with the (110) plane. The reactivity difference between these two surfaces is still not understood.

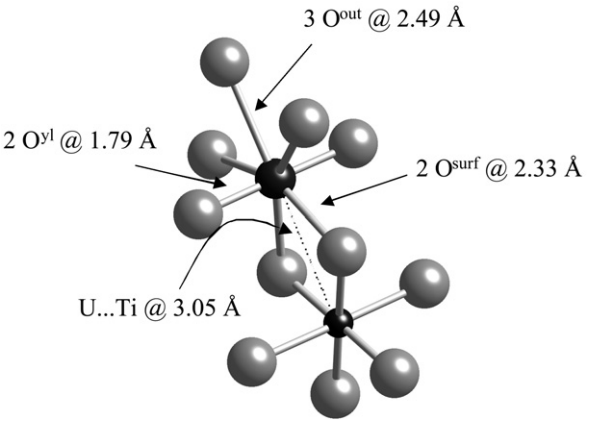

Fig. 7 Site A sorption model onto the (110) surface is shown with the corresponding schematic atomic arrangment according to the best fit parameters of U(VI)/$TiO_2(110)_{//}$.

Acknowledgements

This research was carried out at the Stanford Synchrotron Radiation Laboratory, a national user facility operated by Stanford University on behalf of the U.S. Department of Energy, Office of Basic Energy Sciences, and at the European Synchrotron Radiation Facility. The authors would like to thank for their help J. Bargar and J. Rogers at the SSRL/11-2, T. Reich and A. Bauer at ESRF/ROBL. This work has been financially supported by CEA/bourse Joliot-Curie, PRACTIS (France) and the DOE Office of Basic Energy Science at LANL (USA). Health and Physics operations at SSRL are supported by the Seaborg Institute for Transactinium Science at LANL.

References

1 R. Guillaumont, *Radiochim. Acta*, 1994, **66/67**, 23.
2 C. Degueldre and B. Wernli, *J. Environ. Radioact.*, 1993, **20**, 151.
3 N. Z. Misak, *Colloids Surf. A*, 1995, **97**, 129.
4 S. Nagasaki, S. Tanak, M. Todoriki and A. Suzuki, *J. Alloys Compd.*, 1998, **271/273**, 252.
5 Ch. Papelis and K. Hayes, *Colloids Surf. A*, 1996, **107**, 89.
6 (*a*) T. E. Payne and T. W. Waite, *Radiochim. Acta*, 1991, **52/53**, 487; (*b*) T. E. Payne, J. A. Davis and T. D. Waite, *Radiochim. Acta*, 1996, **74**, 239.
7 J. R. Bargar, R. Reitmeyer, J. J. Lenhart and J. A. Davis, *Geochim. Cosmoschim. Acta*, 2000, **64**, 2737.
8 M. C. Duff, C. Amrhein, P. M. bertsch and D. B. Hunter, *Geochim. Cosmochim. Acta*, 1997, **61**, 73.
9 K. Hayes, Ch. Papeli and J. Leckie, *J. Colloid Interface Sci.*, 1998, **125**, 717.
10 (*a*) N. Marmier, A. Delisee and F. Fromage, *J. Colloid Interface Sci.*, 1999, **211**, 54; (*b*) N. Marmier and F. Fromage, *J. Colloid Interface Sci.*, 1999, **212**, 252.
11 J. S. Noh and J. A. Schwarz, *J. Colloid Interface Sci.*, 1990, **139**, 139.
12 J. R. Bargar, R. Reitmeyer and J. A. Davis, *Environ. Sci. Technol.*, 1999, **33**, 2481.
13 A. J. Dent, J. D. F. Ramsay and S. W. Swanton, *J. Colloid Interface Sci.*, 1992, **150**, 45.
14 R. Drot, E. Simoni and C. Den Auwer, *C. R. Acad. Sci. Paris, Sér. IIc*, 1999, **2**, 111.
15 G. N. Greaves, N. T. Barrett, G. M. Antonini, F. R. Thornley, B. T. M. Willis and A. Steel, *J. Am. Chem. Soc.*, 1989, **111**, 4313.
16 L. N. Moyes, R. H. Parkman, J. M. Charnock, D. J. Vaughan, F. R. Livens, C. R. Hugues and A. Braithwaite, *Environ. Sci. Technol.*, 2000, **34**, 1062.
17 R. J. Reeder, M. Nugent, G. M. Lamble, C. D. Tait and D. E. Morris, *Environ. Sci. Technol.*, 2000, **34**, 638.
18 A. M. Scheidegger, G. M. Lamble and D. L. Sparks, *J. Colloid Interface Sci.*, 1997, **186**, 118.
19 (*a*) S. N. Towle, G. E. Brown and G. A. Parks, *J. Colloid Interface Sci.*, 1999, **217**, 299; (*b*) S. N. Towle, J. R. Bargar, G. E. Brown and G. A. Parks, *J. Colloid Interface Sci.*, 1999, **217**, 312.
20 T. P. Trainor, J. P. Fitts, A. S. Templeton, D. Grolimund and G. E. Jr. Brown, *J. Colloid Interface Sci.*, 2001, **244**, 239.
21 J.-M. Combes, J. Chrisholm-Brause, G. E. Brown, G. A. Parks, S. D. Conradson, P. G. Eller, I. R. Triay, D. E. Hobart and A. Meijer, *Environ. Sci. Technol.*, 1992, **26**, 376.
22 L. N. Moyes, M. J. Jones, W. A. Reed, F. R. Livens, J. M. Charnock, J. F. Mosselmans, C. Henning, D. Vaughan and R. A. Pattrick, *Environ. Sci. Technol.*, 2002, **36**, 179.
23 P. Dähn, A. M. Scheidegger, A. Manceau, E. Curti, B. Baeyens, M. H. Bradbury and D. Chateigner, *J. Colloid Interface Sci.*, 2002, **249**, 8.
24 E. Simoni, R. Drot and C. Den Auwer, unpublished data.
25 T. Reich, G. Bernhard, G. Geipel, H. Funke, C. Henning, A. Rossberg, W. Matz, N. Schell and H. Nitsche, *Radiochim. Acta*, 2000, **88**, 633.
26 J. R. Bargar, G. E. Brown Jr., I. Evans, T. Rabedeau, M. Rowen and J. Rogers, in *Proc. 2nd Euroconference and NEA Workshop on Speciation, Techniques and Facilities for Radioactive Materials at Synchrotron Light Sources*, 2001, Grenoble, France, OECD publication, Paris, France.
27 A. Michalowicz, *J. Phys. IV C2*, 1997, **7**, 235–237 . Available on the LURE web-site www.lure.u-psud.fr.
28 A. L. Ankudinov, B. Ravel, J. J. Rehr and S. D. Conradson, *Phys. Rev. B*, 1998, **58**, 7565.
29 J. J. Rehr and R. C. Albers, *Rev. Mod. Phys.*, 2000, **72**, 621.
30 A. Rosenzweigh and R. R. Ryan, *Am. Mineral.*, 1975, **60**, 448.
31 E. A. Hudson, P. G. Allen, L. J. Terminello, M. A. Denecke and T. Reich, *Phys. Rev. B*, 1996, **54**, 156.
32 E. A. Hudson, J. J. Rehr and J. J. Bucher, *Phys. Rev. B*, 1995, **52**, 13 815.
33 M. O. Kraus and J. H. Oliver, *J. Phys. Chem. Ref. Data*, 1979, **8**, 329.
34 J. Petiau, G. Calas, D. Petimaire, A. Bianconi, M. Benfatto and A. Marcelli, *Phys. Rev. B*, 1986, **34**, 7350.
35 C. Den Auwer, E. Simoni, S. D. Conradson, J. Mustre de Leon, P. Moisy and A. Bérès, *Compt. Rend. Acad. Sci. Paris, Sér. IIc*, 2000, **3**, 327.
36 J. Mustre de Leon, S. D. Conradson, D. L. Clark, C. Den Auwer, N. Hess, D. W. Keogh, P. D. Palmer, E. Simoni and D. Blanchard, to be published.
37 P. H. Citrin, *Phys. Rev. B*, 1985, **31**, 700.
38 D. H. Templeton and L. K. Templeton, *Acta Crystallogr., Sect. A*, 1982, **38**, 62.
39 G. E. Jr. Brown, V. E. Henrich, W. H. Casey, D. L. Clark, C. Eggleston, A. Felmy, D. W. Goodman, M. Grätzel, M. Maciel, M. I. McCarthy, K. H. Nealson, D. A. Sverjensky, M. F. Toney and J. M. Zachara, *Chem. Rev.*, 1999, **99**, 77.
40 P. G. Allen, J. J. Bucher, D. K. Shuh, N. M. Edelstein and T. Reich, *Inorg. Chem.*, 1997, **36**, 4676.
41 P. Charpin, A. Dejean, G. Folcher, P. Rigny and P. Navaza, *J. Chim. Phys. Phys.-Chim. Biol.*, 1985, **82**, 925.
42 C. Chisholm-Brause, S. D. Conradson, C. T. Buscher, P. G. Eller and D. E. Morris, *Geochim. Cosmoschim. Acta*, 1994, **58**, 3625.
43 H. A. Thompson, G. E. Jr. Brown and G. A. Parks, *Am. Mineral.*, 1997, **82**, 483.
44 L. Sémon, C. Boehme, I. Billard, C. Hennig, K. Lützenkirchen, T. Reich, A. Roβberg, I. Rossini and G. Wipff, *ChemPhysChem*, 2001, **2**, 591.
45 V. Vallet, U. Whlgren, B. Schimmelpfennig, H. Moll, Z. Szabo and I. Grenthe, *Inorg. Chem.*, 2001, **40**, 3516.
46 T. D. Waite, J. A. Davis, T. E. Payne, G. A. Waychunas and N. Xu, *Geochim. Cosmochim. Acta*, 1994, **58**, 5465.
47 K. W. Bagnall, in *Comprehensive Coordination Chemistry*, ed. G. Wilkinson, Pergamon Press, Oxford, 1987, vol. 7, ch. 40, and references therein.